ARTICLE

Quantification of Internal Electric Fields and Local Polarization in Ferroelectric Superlattices

Kendra Kathan-Galipeau,[†] Pingping Wu,[‡] Yulan Li,[‡,∥] Long-Qing Chen,[‡] Arsen Soukiassian,[‡,§] Xiaoxing Xi,[‡,⊥] Darrell G. Schlom,[‡,§] and Dawn A. Bonnell[†,*]

[†]Department of Materials Science, The University of Pennsylvania, Philadelphia, Pennsylvania 19104, United States, and [‡]Materials Research Institute, The Pennsylvania State University, University Park, Pennsylvania 16802, United States. [§]Present address: Department of Materials Science and Engineering, Cornell University, Ithaca, NY 14853-1501. [⊥]Present address: Department of Physics, Temple University, Philadelphia, PA 19122. [∥]Present address: Pacific Northwest National Laboratory, Richland, WA 99352.

ABSTRACT Oxide heterostructure superlattices constitute a new family of materials with tunable ferroelectric properties. While theoretical models predict the presence of nanosized ferroelectric domains in these films, they had not been observed as the magnitude of the response functions challenges the limits of experimental detection. Here, a new protocol in a precise variant of piezoforce microscopy is used to image domains in $BaTiO_3$/$SrTiO_3$ superlattices. Comparison of experimentally determined polarization to predictions of phase-field calculations is in quantitative agreement. Additionally, a combination of theory and experiment is used to determine the magnitude of internal electric field within the thin film, in a procedure that can be generalized to all ferroelectric films.

KEYWORDS: PFM · ferroelectric · heterostructure · superlattice · $BaTiO_3$ · phase-field calculation · scanning probe microscopy

Advances in the fabrication of epitaxial oxide thin films and heterostructures, in combination with developments in the theory of complex oxide behavior, have inspired a new class of ferroelectric materials whose properties are controlled by strain and dimensionality.[1−11] The ability to create ferroelectric metamaterials in which ferroelectric and dielectric constituents are combined in epitaxial superlattices with atomic layer thickness precision has enabled fundamental studies of size effects and coupling across interfaces. Quantitative understanding of these phenomena in such superlattices has invoked the presence of domains, though they have up to now not been seen. Here we report the direct observation of domains in epitaxial $BaTiO_3$/$SrTiO_3$ superlattices using a high precision variant of piezoforce microscopy. In addition to imaging the domains, the internal electric field in the films is determined at the nanometer scale. Comparison of experiment to phase-field calculations enables the internal electric field in the thin film to be quantified, which is critical in that it influences the properties of any potential memory, sensing, or switching device based on these materials. These results represent three significant advances: the first imaging of ferroelectric domains in a superlattice, quantification of local polarization, and a new protocol for the determination of the local internal electric field in a ferroelectric film.

In ferroelectric compounds, the coupling between polarization and strain enables strain to be used as a control parameter to tune phase transitions and polarization. Although these effects were first demonstrated using bulk samples, such samples crack at relatively low strains.[12] In contrast, thin films can be commensurately strained to percent levels without fracture *via* mismatch strain to an underlying substrate,[6] enabling enhancement of ferroelectric transition temperatures by hundreds of degrees,[1] the transformation of materials that are normally never ferroelectric into ferroelectrics,[7,13−15] or totally new phenomena to emerge.[16−18] While the effect of strain and dimensionality on macroscopic ferroelectric parameters has been studied, little is known about the effect of strain on ferroelectric domains; indeed many theoretical approaches totally neglect domains.

A widely studied model system of ferroelectric superlattices is $(BaTiO_3)_n/(SrTiO_3)_m$, where n and m refer to the thickness, in unit cells, of the $(001)_p$ $BaTiO_3$ and $(001)_p$ $SrTiO_3$ layers, respectively (Figure 1.) The subscript p refers to pseudocubic indices. This system has been widely investigated by both theory[4,6,19−22] and experiment.[6,20,23,24] Notably, phase-field modeling of the transi-

*Address correspondence to bonnell@lrsm.upenn.edu.

Received for review October 25, 2010 and accepted December 6, 2010.

Published online December 16, 2010. 10.1021/nn102884s

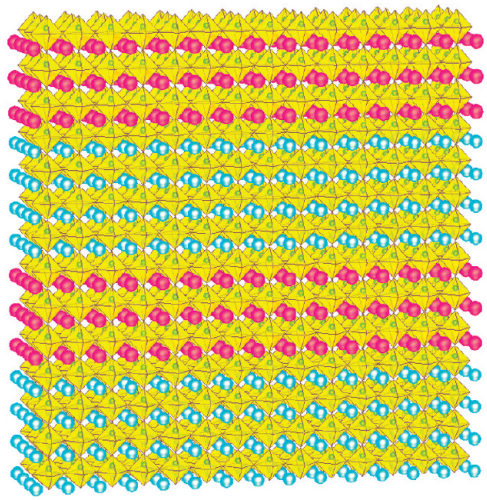

Figure 1. Structure of superlattices. Schematic of the epitaxial $[(BaTiO_3)_3/(SrTiO_3)_4]_{25}$ superlattice grown on a (001) $SrTiO_3$ substrate that was the subject of this study.

tion temperatures of $(BaTiO_3)_n/(SrTiO_3)_m$ superlattices was found to be woefully inaccurate when the films were assumed to be a single domain.[20] Only by assuming that the films split into domains was good agreement between theory and experiment achieved.[20] As no one has reported the observation of domains in any ferroelectric superlattices, including $(BaTiO_3)_n/(SrTiO_3)_m$ superlattices, this raises the important question of whether domains actually exist in these superlattices, which is the subject of this study.

Piezoelectric force microscopy (PFM) is the method of choice for the characterization of domain morphology and switching in ferroelectric materials.[25−28] However, the small domain size and response functions present challenges in relating strain to domain structure in very thin films that are exacerbated in superlattices. The relation between strain and polarization in ferroelectric thin films is determined from laterally macroscopic measurements such as X-ray diffraction, optical second harmonic generation, and more recently Raman spectroscopy.[20,29,30] Consequently, the lateral morphologies of the domains are often not directly determined. Thompson *et al.* have used electrostatic force imaging (or surface potential) of epitaxial $PbTiO_3$ thin films to map changes in domain morphology, providing a visualization of domains.[31] This approach is effective in characterizing domain morphology and, in some cases, domain dynamics but does not yield properties, such as polarization. To date, the small piezoelectric strains and nanometer size of ferroelectric domains associated with thin film heterostructure geometries have precluded quantitative application to this problem. Here we combine dual resonant tracking in piezoelectric force microscopy (PFM) with pixel-by-pixel normalization to allow picometer piezoelectric responses in nanometer sized domains to be quantified. It is well-known that this approach is susceptible to topographic cross-talk, so we analyze only surfaces with roughness less than 0.2 nm and where no cross-talk is detected.

Figure 2 compares the topographic structure and amplitude images of three different thin films which have different domain morphologies. The films are extremely flat in most areas with roughness <1 nm over 1 μm^2 area. Analysis was carried out in areas with topographic variation less than 0.2 nm. In regions where topographic features were larger, or similar features appeared in the amplitude image, further analysis was not attempted. In dual resonance tracking PFM, the measured parameters are amplitudes (A_1, A_2) and phases (ϕ_1, ϕ_2) at each of two frequencies (f_1, f_2), one above and one below the resonance. Feeding back on the differences at these two frequencies does much to minimize the effect of variations in local contact resonance. How-

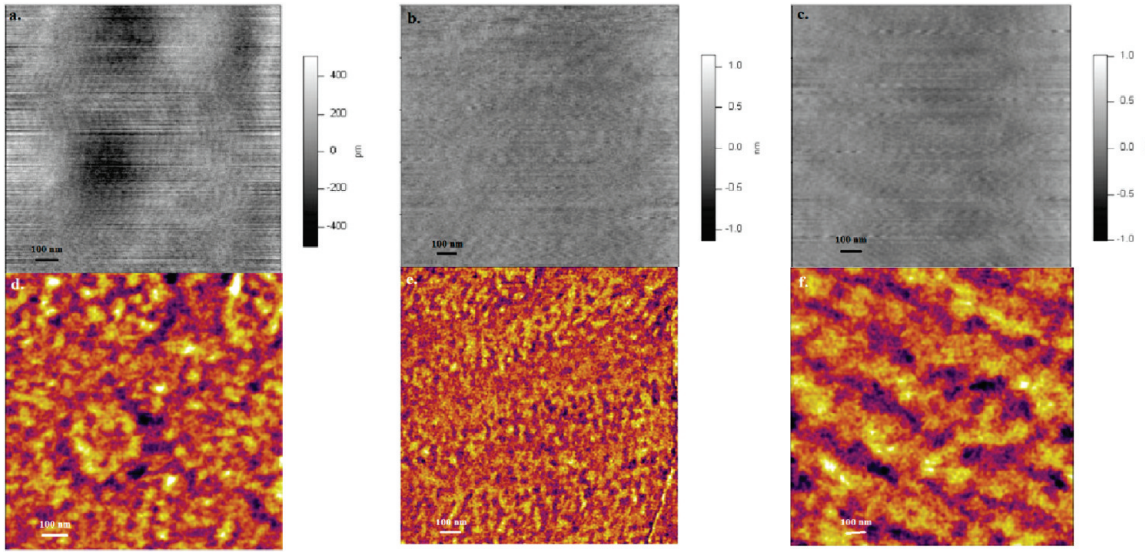

Figure 2. Topography and amplitude (polarization) images of BTO/STO heterostructures grown on three substrates. (a−c) Topography images. (d−f) Amplitude images. a,d = $SrTiO_3$ (compression); b,e = $GdScO_3$ (relaxed); c,f = $SmScO_3$ (tension); (a−c) 1 μm scan sizes. *Z* range for d−f = 1.5 pm.

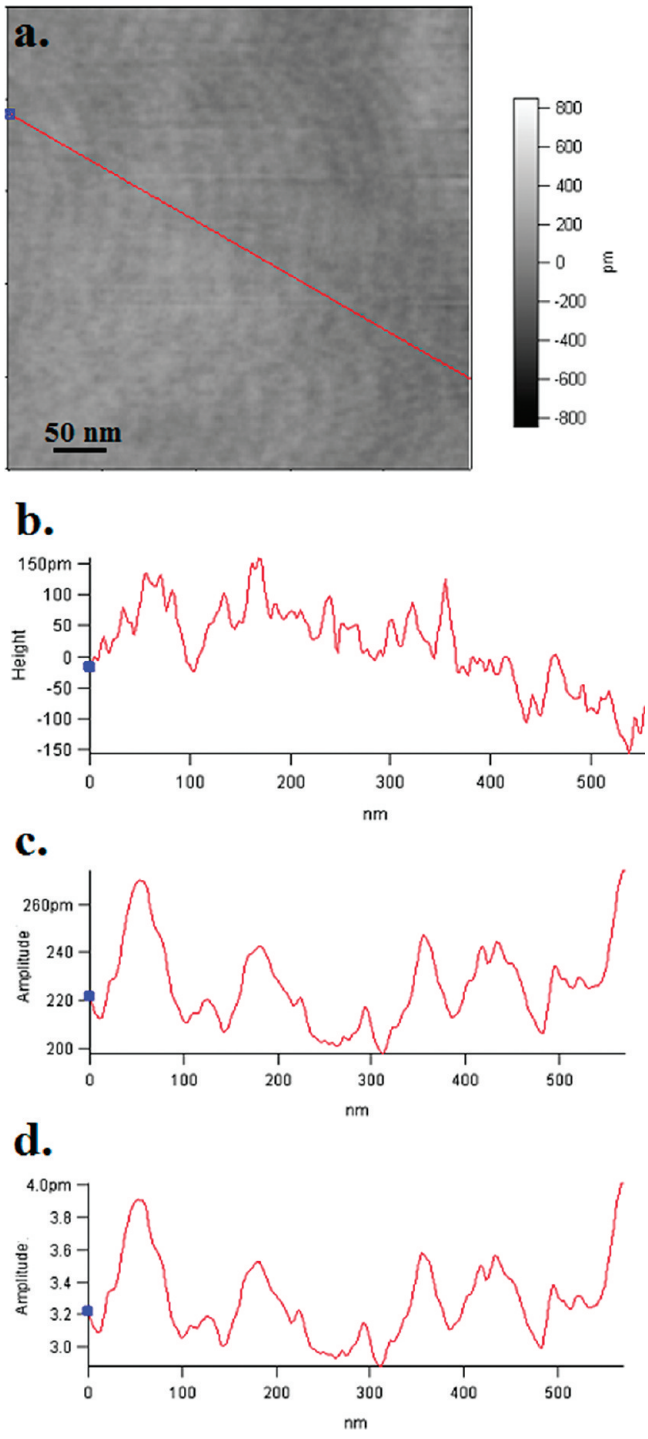

Figure 3. $BaTiO_3/SrTiO_3$ heterostructures grown on a (100) $SrTiO_3$ (a) topographic image, (b) line profile of topography, (c) line profile of raw amplitude (polarization), (d) line profile of corrected amplitude (polarization).

ever, it does not yield a sample response independent of the contact resonance, specifically it does not yield the exact resonance frequency, f_0, and quality factor, Q. Gannepalli *et al.*[32] developed an analytical description based on a damped oscillator model that isolates these as follows.

The measured amplitude (A_i where $i = 1$ or 2), which includes the contact resonance, is related to the actual amplitude of the surface, A_{drive}, as

$$A_i = \frac{A_{drive} f_0^2}{\sqrt{(f_0^2 - f_i^2)^2 + (f_0 f_i/Q)^2}}$$

where A_{drive}, f_0, and Q are unknown and A_i and f_1, f_2 are experimentally known.

$$f_0 = \sqrt{f_1 f_2 \frac{f_2 X_1 - f_1 X_2}{f_1 X_1 - f_2 X_2}}$$

$$Q = \frac{\sqrt{f_1 f_2 (f_2 X_1 - f_1 X_2)(f_1 X_1 - f_2 X_2)}}{f_2^2 - f_1^2}$$

where

$$X_1 = -\frac{1 - sgn(\beta)\alpha\sqrt{1 + \beta^2}}{\beta}$$

$$X_2 = -\frac{1 - sgn(\beta)\sqrt{1 + \beta^2}/\alpha}{\beta}$$

and

$$\alpha = \frac{f_1 A_1}{f_2 A_2}$$

$$\beta = \tan(\tilde{\varphi}_2 - \tilde{\varphi}_1)$$

Using these relations, the measured amplitudes and phases along with the frequency set points can be used to calculate the actual Q and f_0 at every pixel in the image. This in turn yields the response of the sample, independent of the contact resonance of the cantilever. Figure 3 compares the topographic signal in a region on a $BaTiO_3/SrTiO_3$ heterostructure with a usual amplitude signal and the "corrected" value of sample response. Two important observations are that the PFM amplitude and surface topography differ and that the corrected amplitude differs from the measured amplitudes. Note that while it is possible to image surface variations associated with domains in the absence of the normalization, the corrections are necessary to quantify the polarization in ferroelectric superlattices. The thin film geometry is critical to the analysis as it provides an ideal configuration in that local electric fields induced by the tip are, to first order, linear through the film, which is in contrast to the general case of thicker samples.[33] In addition, the crystallographic orientation constrains the polarization vectors to be within the plane of the film or perpendicular to the surface.

Figure 4 illustrates the polarization variation in a $BaTiO_3/SrTiO_3$ superlattice in which the film is in compression, so the domains are perpendicular to the surface. Figure 4a,b shows that the morphology consists of meandering domains with sizes ranging from 50 to 100 nm. The piezoresponse amplitudes (Figure 4c) exhibit two peaks centered around 2.3 and 2.6 pm that correspond to 0.57 and 0.65 pm/V and are attributed to up-

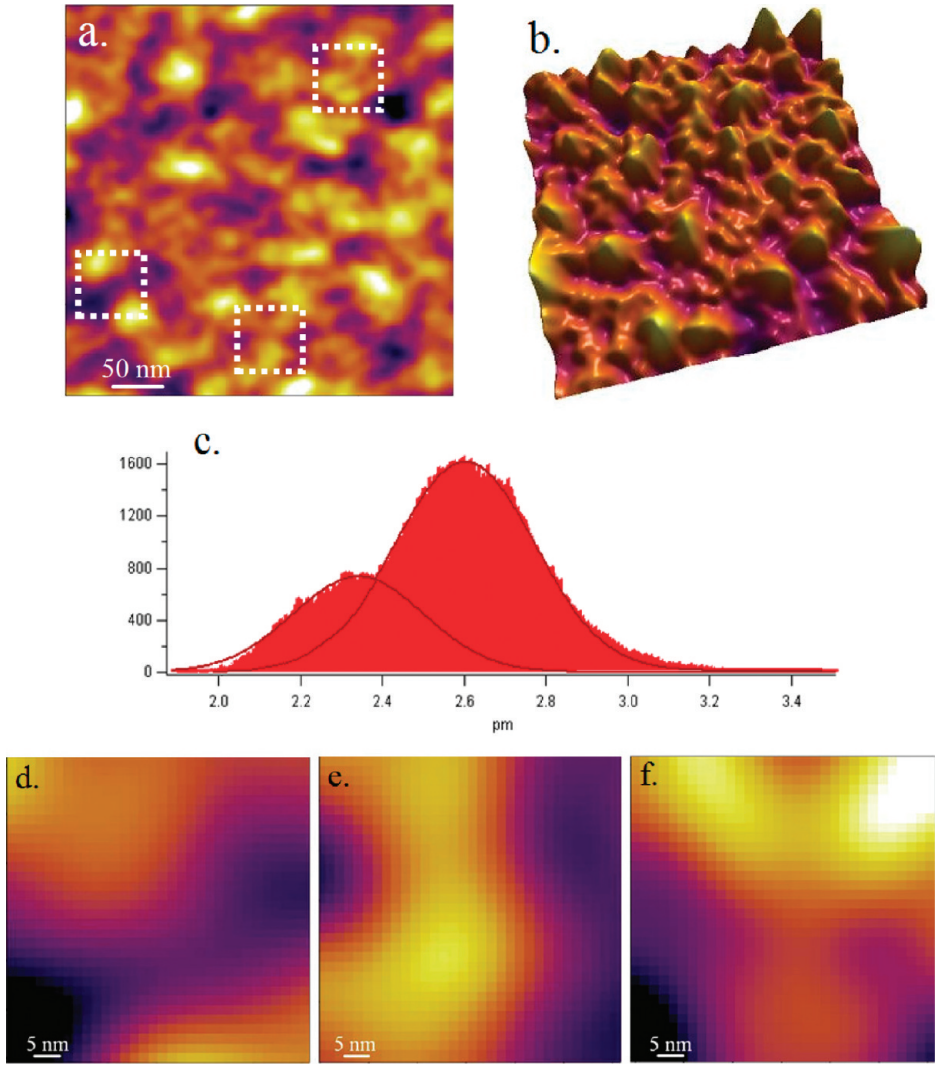

Figure 4. Polarization of superlattices. Amplitude (polarization) images of $BaTiO_3/SrTiO_3$ heterostructures grown on a (100) $SrTiO_3$ substrate. Large area scans showing variations of piezoresponse (a,b), distribution of piezoresponse between 2.0 and 3.2 pm with the lines as a guide to the eye (c), subsets of the same dimensions as the simulation cell (d−f). Images acquired with tip-free resonance = 79.14 kHz, k = 2.23 N/m, deflection set point = 0.3 V, oscillation amplitude = 6.6 V, tip contact resonance = 312.1 kHz, amplitude offset = 4 kHz; (b) 500 nm × 500 nm image. Z range for a,b = 1.5 pm and d−f = 1 pm.

ward c+ and downward c− orientated domains. (The line is simply a guide for the eye and not analytical.) Since the tip diameter is ~30 nm, which is on the same order as that of the domains, the tip is often over more than one domain; therefore, the maxima and minima values most accurately reflect the piezoresponse of the domains. The ratio of the amplitudes of the c+ and c− domains is about 1.2, which is discussed in detail below.

The ferroelectric domain morphologies are predicted by the phase-field method coupled with microelasticity and electrostatics.[34,35] Figure 5a,b shows the calculated domain structures of the $BaTiO_3$ layer and $SrTiO_3$ layer within a $(BaTiO_3)_3/(SrTiO_3)_4$ superlattice on $SrTiO_3$. If we assume that the superlattice is fully commensurate with substrate $SrTiO_3$, and at room temperature $a_{sub}(SrTiO_3)$ = 3.905 Å, the BTO layer $a_{sup}(BaTiO_3)$ = 4.005 Å within the superlattice is subject to a strain of $e_{11} = e_{22} = -2.5\%$, while the $SrTiO_3$ layers are not strained. Figure 5 compares the $SrTiO_3$- and $BaTiO_3$-terminated surfaces and shows the dimension of the internal layer of the heterostructure. Note that the $BaTiO_3$ layer is thinner than the $SrTiO_3$ layer, as in the experimental superlattice. Surprisingly, both layers are polarized with relatively large (40−100 nm) tetragonal phase c+/c− domains. The size and general shape of the domains agree well with experiment. The polarization in the $BaTiO_3$ layer is spontaneous, while that in the $SrTiO_3$ layer is induced by the polarization in the $BaTiO_3$ layer to decrease the electrostatic energy. The induced polarization in the $SrTiO_3$ is of the same orientation as that in the $BaTiO_3$ so Figure 5a,b exhibits the same terminations. This is, however, not the case for films with different strain conditions.

A film consisting entirely of c+ and c− domains should exhibit no variations in piezoresponse except

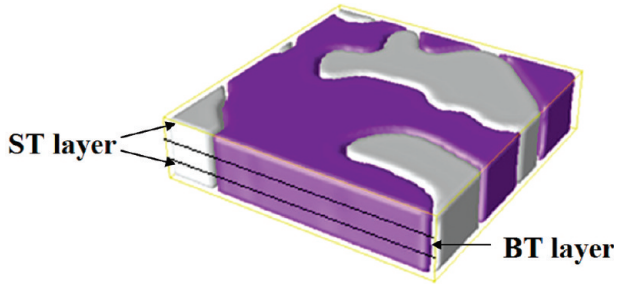

Figure 5. Calculated polarization. Phase-field calculations of the ferroelectric domain structure in a $(BaTiO_3)_3/(SrTiO_3)_4$ superlattice constrained to the lattice constant of the underlying (001) $SrTiO_3$ substrate showing the domain structure of the $SrTiO_3$ layer on the surface. The size of the calculated image is 64 nm × 64 nm × 2.8 nm, but the *z* axis is exaggerated in order to illustrate the locations of the layers in the film. The $BaTiO_3$ layer is in the center of the slab with the $SrTiO_3$ at the outer surfaces. The calculation with the $BaTiO_3$ layer at the surface looks exactly the same.

at the domain boundaries. However, Figure 4 shows that there is a clear difference in the measured response over c+ and c− domains. Ferroelectric films often contain internal electric fields; they are a consequence of differences in boundary conditions at the top and bottom surfaces, which result in polarization asymmetry. In order to examine this possibility, an electric field was included in the phase-field simulation by introducing the electrostatic energy $F_{elec} = -E_iP_i$; only a minor difference was observed in the domain structure. The internal field dependence of the ratio of the average of the x_3 component of the polarization vector, positive and negative, respectively, (Ave. P_z+)/(Ave. P_z−) is shown in Figure 6.

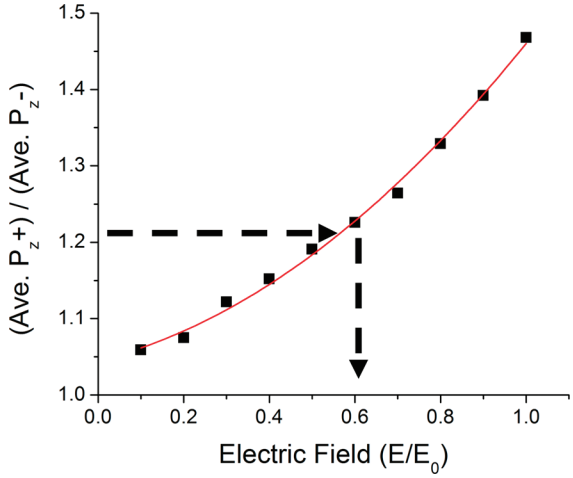

Figure 6. Determining the internal electric field. The ratio of the average of the x_3 component of the positive and negative polarization vector, *i.e.*, (Ave. P_z+)/(Ave. P_z−), at different internal electrical field, predicted by phase-field simulation, where $E_0 = 9.65 \times 10^6$ V/m in the simulation. The dotted lines show the experimentally determined polarization asymmetry and consequent internal field.

The polarization asymmetry is proportional to the internal electrical field. The experimentally observed asymmetry is predicted to occur with a field of ~5.7×10^6 V/m (around $0.6E_0$ in the theory prediction, where $E_0 = 9.65 \times 10^6$ V/m). (See the Methods section for the justification of these values.) The field is well below (10−30% of E_c) the expected coercive field for epitaxial films of the thicknesses in these devices.[36−40] The presence of an internal field implies differences in polarization compensation mechanisms at the bottom electrode and at the surface. If under the ambient conditions used here the surface is completely compensated by atmospheric adsorbates, then the variations can be attributed to the film/substrate interface. For example, the substrate may more effectively supply carriers of one sign for compensation, leading to an opposite charge at this interface. More work is required to isolate the origins of the charge. Note that while the results in Figure 4 distinguish the differences in domain properties, a measurement with electrodes larger than the domain size (10−20 nm) would determine the polarization to be an intermediate value, ~0.6 pm/V, reflecting the behavior of neither.

In summary, we have experimentally determined the value of polarization and domain structure in ferroelectric $BaTiO_3/SrTiO_3$ superlattices. The morphology of the nanometer sized domains is in exceptionally good agreement with theoretical calculations. Furthermore, the directional asymmetry in the observed polarization was used to estimate the internal electric field in the film. This approach to high precision characterization of small piezoresponses can lead to better characterization of ferroelectric thin films. Perhaps more importantly, the protocol that exploits these precise measurements in conjunction with theoretical calculations to determine internal electric fields locally can be generalized.

METHODS

Dual Frequency Piezoelectric Force Microscope. In PFM, an ac electric field is applied to a conducting probe tip on a surface, and the resulting expansion/contraction due to the inverse piezoelectric effect piezoresponse is quantified from the mechanical response of the cantilever. Signal to noise is enhanced by operating near the resonance of the cantilever in contact with the surface (the so-called contact resonance). The contact resonance is known to vary with position on a surface, an effect that is usually ignored. In dual frequency PFM, a frequency above and one below the resonance are excited.[40] Both amplitudes are detected and used to shift frequencies so that contact resonance variations are eliminated from the data. In addition, we correct each pixel with an analytical model that separates the contact resonance and the sample response function.[32] Images were acquired with tip-free resonance = 79.14 kHz, k = 2.23 N/m, deflection set point = 0.3 V, oscillation amplitude = 6.6 V, tip contact resonance = 312.1 kHz, and amplitude offset = 4 kHz. Nonlocal electrostatic contributions were estimated with Si control samples and shown to have noise on the order of 140 fm.

Film Growth. An epitaxial $(BaTiO_3)_3/(SrTiO_3)_4$ superlattice consisting of three unit cells of $(001)_p$ $BaTiO_3$ followed by four unit cells of $(001)_p$ $SrTiO_3$, repeated 25 times was grown on a (001) TiO_2-terminated[41] $SrTiO_3$ substrate by reactive molecular-beam

epitaxy (MBE). The configuration is illustrated in Figure 1. The $BaTiO_3/SrTiO_3$ superlattice was formed by sequential shuttered deposition of the precise single-monolayer doses of BaO, SrO, and TiO_2 at substrate temperature of ~650 °C and a background pressure of 5×10^{-7} Torr of molecular oxygen. Growth was initiated with the SrO monolayer of the four unit cell thick $(001)_p$ $SrTiO_3$ layer and ended with the TiO_2 monolayer of the three unit cell thick $(001)_p$ $BaTiO_3$ layer. Four-circle X-ray diffraction analysis confirmed that the $[(BaTiO_3)_3/(SrTiO_3)_4]_{25}$ superlattice sample was commensurate with the underlying substrate (see Supporting Information). The details of the shuttered reflection high-energy electron diffraction (RHEED) intensity oscillations used to control film stoichiometry and the unit cell layer thicknesses of the $BaTiO_3$ and $SrTiO_3$ layers as well as structural characterization of other $BaTiO_3/SrTiO_3$ superlattices grown in the same way can be found in ref 23.

Phase-Field Calculations. The ferroelectric domain structures are predicted by the phase-field method coupled with microelasticity and electrostatics.[34,35] In this approach, we use the polarization $\boldsymbol{P}(\boldsymbol{x}) = [P_1(\boldsymbol{x}), P_2(\boldsymbol{x}), P_3(\boldsymbol{x})]$, as order parameter, and its temporal evolution, thus the domain structure, is described by the time-dependent Ginzburg−Landau (TDGL) equations

$$\frac{\partial P_i(\boldsymbol{x}, t)}{\partial t} = -L\frac{\delta F}{\delta P_i(\boldsymbol{x}, t)} \quad (i = 1, 2, 3) \tag{1}$$

where $\boldsymbol{x} = (x_1, x_2, x_3)$ is the coordinate, t is time, L is the kinetic coefficient related to the ferroelectric domain wall mobility, and F is the total free energy of the system, which is given by

$$F = F_{bulk}(P_i) + F_{elas}(P_i, \varepsilon_{ij}) + F_{elec}(P_i, E_i) + F_{grad}(P_{i,j}) \tag{2}$$

where F_{bulk}, F_{elas}, F_{elec}, and F_{grad} are the bulk chemical, elastic, electrostatic, and gradient energies, respectively, ε_{ij} is the elastic strain, E_i is the electric field components induced from dipole−dipole interactions, and $P_{i,j} = \partial P_i/\partial x_j$. The mathematical expressions and the numerical coefficients for obtaining the different energy contributions can be found in ref 21. The cell grid matrix employed in our phase-field model is $(64\Delta x_1 \times 64\Delta x_2) \times N\Delta x_3$, where the $\Delta x_1 = \Delta x_2 = 1$ nm, $\Delta x_3 = 0.5a_{sub}(SrTiO_3) = 0.5 \times 0.3905$ nm, $N = 2(n + m)$ for a $(BaTiO_3)_n/(SrTiO_3)_m$ structure. We assume that the top surface of the superlattice and the film/substrate interface are charge-compensated along the x_3 direction and model the superlattice as a periodic structure. In the simulation, the in-plane strains, e_{11} and e_{22}, imposed on the superlattice are calculated from the lattice parameter difference:

$$e_{11} = e_{22} = \frac{a_{sub} - a_{sup}}{a_{sup}} \tag{3}$$

where a_{sub} and a_{sup} is the lattice parameter of the substrate and superlattice.

In our simulations, all quantities are converted to dimensionless quantities, and at the end of a simulation, we convert them back to values in real units. For example, 0.26 C/m is the spontaneous polarization of $BaTiO_3$ at room temperature, and it is used to normalize the polarization. In a simulation, if the local polarization value is 0.5, it means it is 0.5 × 0.26 C/m in real units; a_1 is the Landau coefficient for $BaTiO_3$ for the second-order term. Using those quantities to do reduced units, the conversion factor from values (in reduced unit, *i.e.*, dimensionless) to values with real unit for electric field is E_0. So if the electric field in the simulation is 0.8, it is $0.8 \times E_0$ in real units.

Acknowledgment. We gratefully acknowledge helpful discussions with K. Jones and A. Gannepalli. This research was partially supported by the National Science Foundation Ceramics Division DMR-0805174 with facilities support from the Nano/Bio Interface Center, NSEC DMR-0832802. We also gratefully acknowledge the financial support from the National Science Foundation through Grant No. DMR-0507146 and the MRSEC program (Grant No. DMR-0820404).

Supporting Information Available: Structural characterization of $[(BaTiO_3)_3/(SrTiO_3)_4]_{25}$ superlattice. This material is available free of charge *via* the Internet at http://pubs.acs.org.

REFERENCES AND NOTES

1. Pertsev, N. A.; Zembilgotov, A. G.; Tagantsev, A. K. Effect of Mechanical Boundary Conditions on Phase Diagrams of Epitaxial Ferroelectric Thin Films. *Phys. Rev. Lett.* **1998**, *80*, 1988–1991.
2. Warusawithana, M.; Colla, E. V.; Eckstein, J. N.; Weissman, M. B. Artificial Dielectric Superlattices with Broken Inversion Symmetry. *Phys. Rev. Lett.* **2003**; 03680.
3. Dawber, M.; Lichtensteiger, C.; Cantoni, M.; Veithen, M.; Ghosez, P.; Johnston, K.; Rabe, K. M.; Triscone, J.-M. Unusual Behavior of the Ferroelectric Polarization in $PbTiO_3/SrTiO_3$ Superlattices. *Phys. Rev. Lett.* **2005**, *95*, 177601.
4. Dawber, M.; Rabe, K. M.; Scott, J. F. Physics of Thin-Film Ferroelectric Oxides. *Rev. Mod. Phys.* **2005**, *77*, 1083–1130.
5. Lee, H. N.; Christen, H. M.; Chisholm, M. F.; Rouleau, C. M.; Lowndes, D. H. Strong Polarization Enhancement in Asymmetric Three-Component Ferroelectric Superlattices. *Nature* **2005**, *433*, 395.
6. Schlom, D. G.; Chen, L.-Q.; Eom, C.-B.; Rabe, K. M.; Streiffer, S. K.; Triscone, J. M. Strain Tuning of Ferroelectric Thin Films. *Annu. Rev. Mater. Res.* **2007**, *37*, 589–626.
7. Bousquet, E.; Dawber, M.; Stucki, N.; Lichtensteiger, C.; Hermet, P.; Gariglio, S.; Triscone, J.-M.; Ghosez, P. Improper Ferroelectricity in Perovskite Oxide Artificial Superlattices. *Nature* **2008**, *452*, 732.
8. Specht, E. D.; Christen, H. M.; Norton, D. P.; Boatner, L. A. X-ray Diffraction Measurement of the Effect of Layer Thickness on the Ferroelectric Transition in Epitaxial $KTaO_3/KNbO_3$ Multilayers. *Phys. Rev. Lett.* **1998**, *80*, 4317–4320.
9. Tenne, D. A.; Turner, P; Schmidt, J. D.; Biegalski, M.; Li, Y. L.; Chen, L. Q.; Soukiassian, A.; Trolier-McKinstry, S.; Schlom, D. G.; Xi, X. X.; *et al.* Ferroelectricity in Ultrathin $BaTiO_3$ Films: Probing the Size Effect by Ultraviolet Raman Spectroscopy. *Phys. Rev. Lett.* **2009**, *103*, 177601.
10. Kukhar, V. G.; Pertsev, N. A.; Kholkin, A. L. Thermodynamic Theory of Strain-Mediated Direct Magnetoelectric Effect in Multiferroic Film−Substrate Hybrids. *Nanotechnology* **2010**, *21*, 265701.
11. Borisevich, A. Y.; Chang, H. J.; Huijben, M.; Oxley, M. P.; Okamoto, S.; Niranjan, M. K.; Burton, J. D.; Tysmbal, E. Y.; Chu, Y. H.; Yu, P.; *et al.* Suppression of Octahedral Tilts and Associated Changes in Electronic Properties at Epitaxial Oxide Heterostructure Interfaces. *Phys. Rev. Lett.* **2010**, *105*, 027201.
12. Forsburgh, J. P.W. Effect of a Two-Dimensional Pressure on the Curie Point of Barium Titanate. *Phys. Rev.* **1954**, *93*, 686–692.
13. Pertsev, N. A.; Tagantsev, A. K.; Setter, N. Phase Transitions and Strain-Induced Ferroelectricity in $SrTiO_3$ Epitaxial Thin Films. *Phys. Rev. B* **2000**, *61*, 825–829.
14. Haeni, J. H.; Irvin, P.; Chang, W.; Uecker, R.; Reiche, P.; Li, Y. L.; Choudhury, S.; Tian, W.; Hawley, M. E.; Craigo, B.; *et al.* Room Temperature Ferroelectricity in Strained $SrTiO_3$. *Nature* **2004**, *430*, 758–761.
15. Tyunina, M.; Narkilahti, J.; Plekh, M.; Oja, R.; Nieminen, R. M.; Dejneka, A.; Trepakov, V. Evidence for Strain-Induced Ferroelectric Order in Epitaxial Thin-Film $KTaO_3$. *Phys. Rev. Lett.* **2010**, *104*, 227601.
16. Lee, J. H.; Rabe, K. M. Epitaxial-Strain-Induced Multiferroicity in $SrMnO_3$ from First Principles. *Phys. Rev. Lett.* **2010**, *104*, 207204.
17. Lee, J. H.; Fang, L.; Vlahos, E.; Ke, X.; Jung, Y. W.; Fitting Kourkoutis, L.; Kim, J. W.; Ryan, P.; Heeg, T.; Roeckerath, M.; *et al.* A Strong Ferroelectric Ferromagnet Created By Means of Spin-Lattice Coupling. *Nature* **2010**, *466*, 954–958.
18. Fennie, C. J.; Rabe, K. M. Magnetic and Electric Phase Control in Epitaxial $EuTiO_3$ from First Principles. *Phys. Rev. Lett.* **2006**, *97*, 267602.

19. Neaton, J. B.; Rabe, K. M. Theory of Polarization Enhancement in Epitaxial $BaTiO_3/SrTiO_3$ Superlattices. *Appl. Phys. Lett.* **2003**, *82*, 1586–1588.
20. Tenne, D. A.; Bruchhausen, A.; Lanzillotti-Kimura, N. D.; Fainstein, A.; Katiyar, R. S.; Cantarero, A.; Soukiassian, A.; Vaithyanathan, V.; Haeni, J. H.; Tian, W.; *et al.* Probing Nanoscale Ferroelectricity by Ultraviolet Raman Spectroscopy. *Nature* **2006**, *313*, 1614.
21. Li, Y. L.; Hu, S. Y.; Tenne, D.; Soukiassian, A.; Schlom, D. G.; Xi, X. X.; Choi, K. J.; Eom, C. B.; Saxena, A.; Lookman, T.; *et al.* Prediction of Ferroelectricity in $BaTiO_3/SrTiO_3$ Superlattices with Domains. *Appl. Phys. Lett.* **2007**, *91*, 112914.
22. Li, Y. L.; Hu, S. Y.; Tenne, D.; Soukiassian, A.; Schlom, D. G.; Chen, L. Q.; Xi, X. X.; Choi, K. J.; Eom, C. B.; Saxena, A.; *et al.* Interfacial Coherency and Ferroelectricity of $BaTiO_3/SrTiO_3$ Superlattice Films. *Appl. Phys. Lett.* **2007**, *91*, 252904.
23. Soukiassian, A.; Tian, W.; Vaithyanathan, V.; Haeni, J. H.; Chen, L.-Q.; Xi, X. X.; Schlom, D. G.; Tenne, D. A.; Sun, H. P.; Pan, X. Q.; *et al.* Growth of Nanoscale $BaTiO_3/SMO_3$ Superlattices by Molecular-Beam Epitaxy. *J. Mater. Res.* **2008**, *23*, 1417.
24. Iijima, K.; Terashima, T.; Bando, Y.; Kamigaki, K.; Terauchi, H. Atomic Layer Growth of Oxide Thin Films with Perovskite-Type Structure by Reactive Evaporation. *J. Appl. Phys.* **1992**, *72*, 2840.
25. Kalinin, S. V., Gruverman, A., Eds. *Scanning Probe Microscopy of Electrical and Electromechanical Phenomena at the Nanoscale*; Springer: Berlin, 2007.
26. Hong, S. *Nanoscale Phenomena in Ferroelectric Thin Films*; Kluwer: Dordrecht, The Netherlands, 2004.
27. Polomoff, N. A.; Premnath, R. N.; Bosse, J. L.; Huey, B. D. Ferroelectric Domain Switching Dynamics with Combined 20 nm and 10 ns Resolution. *J. Mater. Sci.* **2009**, *44*, 5189–5196.
28. Klein, L. J.; Dubourdieu, C.; Frank, M. M.; Hoffman, J.; Reiner, J. W.; Ahn, C. H. Domain Dynamics in Epitaxial $Pb(Zr_{0.2}Ti_{0.8})O_3$ Films Studied by Piezoelectric Force Microscopy. *J. Vac. Sci. Technol., B* **2010**, *28*, C5A20–C5A23.
29. Choi, K. J.; Biegalski, M.; Li, Y. L.; Sharan, A.; Schubert, J.; Uecker, R.; Reiche, P.; Chen, Y. B.; Pan, X. Q.; Gopalan, V.; *et al.* Enhancement of Ferroelectricity in Strained $BaTiO_3$ Thin Films. *Science* **2004**, *306*, 1005.
30. Streiffer, S. K.; Eastman, J. A.; Fong, D. D.; Thompson, C.; Munkholm, A.; Ramana Murty, M. V.; Auciello, O.; Bai, G. R.; Stephenson, G. B. Observation of Nanoscale 180 Degree Stripe Domains in Ferroelectric $PbTiO_3$ Thin Films. *Phys. Rev. Lett.* **2002**, *89*, 067601.
31. Thompson, C.; Fong, D. D.; Wang, R. V.; Jiang, F.; Streiffer, S. K.; Latifi, K.; Eastman, J. A.; Fuoss, P. H.; Stephenson, G. B. Imaging and Alignment of Nanoscale 180 Degree Stripe Domains in Ferroelectric Thin Films. *Appl. Phys. Lett.* **2008**, *93*, 182901.
32. Gannepalli, A.; Yablon, D.; Proksch, R. Dual AC Resonance Tracking Imaging of Nanoscale Elasticity and Dissipation. In *International Workshop on SPM for Energy Applications*, **2010**.
33. Kalinin, S. V.; Morozovska, A. N.; Chen, L. Q.; Rodriguez, B. J. Local Polarization Dynamics in Ferroelectric Materials. *Rep. Prog. Phys.* **2010**, *73*, 056502.
34. Li, Y. L.; Hu, S. Y.; Liu, Z. K.; Chen, L. Q. Phase-Field Model of Domain Structures in Ferroelectric Thin Films. *Appl. Phys. Lett.* **2001**, *78*, 3878.
35. Li, Y. L.; Hu, S. Y.; Liu, Z. K.; Chen, L. Q. Effect of Substrate Constraint on the Stability and Evolution of Ferroelectric Domain Structures in Thin Films. *Acta Mater.* **2002**, *50*, 395.
36. Zanetti, S. M.; Buero, P. R.; Leite, E.; Longo, E.; Varela, J. A. Ferroelectric and Microstructural Characteristics of $SrBi_2Ta_2O_9$ Thin Films Crystallized by the Rapid Thermal Annealing Process. *J. Appl. Phys.* **2001**, *89*, 3416–3419.
37. Choudhury, S.; Li, Y. L.; Chen, L. Q.; Jia, Q. X. Strain Effect on Coercive Field of Epitaxial Barium Titanate Thin Films. *Appl. Phys. Lett.* **2008**, *92*, 142907.
38. Jo, J. Y.; Kim, Y. S.; Noh Jong-Gul Yoon, T. W. Coercive Fields in Ultrathin $BaTiO_3$ Capacitors. *Appl. Phys. Lett.* **2006**, *89*, 232909.
39. Abe, K. K. S.; Yanase, N.; Kawakubo, T. Asymmetric Ferroelectricity and Anomalous Current Conduction in Heterepitaxial $BaTiO_3$ Thin Films. *Jpn. J. Appl. Phys.* **1997**, *36*, 5846–5853.
40. Rodriguez, B. J.; Callahan, C.; Kalinin, S. V. Dual Frequency Resonance Tracking Atomic Force Microscopy. *Nanotechnology* **2007**, *18*, 475504.
41. Koster, G.; Kropman, B. L.; Rijnders, G. J. H. M.; Blank, D. H. A. Quasi-Ideal Strontium Titanate Crystal Surfaces through Formation of Strontium Hydroxide. *Appl. Phys. Lett.* **1998**, *73*, 2920.